Peer-reviewed version available at *Sensors* **2018**, *18*, 2597; doi:10.3390/s18082597

Article

Distributed deformation monitoring for a single-cell box girder based on distributed long-gage fiber bragg grating (LFBG) sensors

Sheng Shen[1,2]* and Shao-fei Jiang[1]

[1] Department of civil engineering, Fuzhou University, Fuzhou, Fujian 350108, China; s_shen@126.com; cejsf@fzu.edu.cn
[2] Hebei Province Key Laboratory of Evolution and Control of Mechanical Behavior in Traffic Engineering Structure (Shijiazhuang Tiedao University), Shijiazhuang Tiedao University, Shijiazhuang, Hebei 050043, China; s_shen@126.com
* Correspondence: s_shen@126.com; Tel.: +86-0591-2286-5379

Abstract: Distributed deformation based on Fiber Bragg Grating sensors or other kinds of strain sensors can be used to evaluate safety in operating periods of bridges. However, most of the published researches about distributed deformation monitoring are focused on solid rectangular beam rather than box girder—a kind of typical hollow beam widely employed in actual bridges. Considering that the entire deformation of a single-cell box girder contains not only bending deflection but also two additional deformations respectively caused by shear lag and shearing action, this paper again revises the improved conjugated beam method (ICBM) based on the LFBG sensors to satisfy the requirements for monitoring two mentioned additional deformations. The best choice for the LFBG sensor placement in box gilder is also proposed in this paper due to strain fluctuation on flange caused by shear lag effect. Results from numerical simulations show that most of the theoretical monitoring errors of the revised ICBM are 0.3%~1.5%, and the maximum error is 2.4%. A loading experiment for a single-cell box gilder monitored by LFBG sensors show that most of the practical monitoring errors are 6%~8%, and the maximum error is 11%.

Keywords: deformation monitoring; distributed monitoring; single-cell box girder; long-gage strain; long-gage Fiber Bragg Grating; strain distribution; shear lag effect; shear action

1. Introduction

Monitored deformation is usually used as an effective index not only to evaluate the overall health and safety of the in-service bridges but also to prevent some abnormal states due to the inextricable relationship between the deformation and the stress/strain distribution. Geodetic survey using digital level or total station has been widely applied to directly measuring bridge deformation [1,2] because of its low cost and easy operation. The main disadvantages of geodetic survey are possible obstruction to public traffic when the survey is ongoing and measurement error from manual observation. Recently, some automatic monitoring techniques, such as Global Positioning System [3,4], displacement sensors[5], hydrostatic leveling system[6] and laser measurements[7] are applied to gain bridge deformation. However, these sensors may be also disturbed by some environmental factors including bad weather, accidental vibration or satellite ephemeris error. In addition, these techniques used in deformation monitoring are criticized as the characteristics of "point" sensing, which implies that they can only collect displacements of a few predesigned points. In practical monitoring, these "point" sensing techniques may ignore some damages occurred in other positions. Therefore, installing large numbers of "point" sensors to obtain distributed deformation may result in cost overruns in long-term monitoring. The best solution to keep balance between comprehensive monitoring and its cost is to replace these "point" sensors with some kind of distributed sensors.

In recent years, some indexes including slope variation [8] or strain distribution [9] before or after applied loads are introduced to indirectly calculate bridge deformation. Considering that the slope is the first derivative of bending deflection in an Euler–Bernoulli beam, an n degree polynomial used to approximate to the bridge deflection can be differentiated once to an n-1 degree polynomial. Then the n monitored slopes and their position coordinates can be substituted to the n-1 degree polynomial to form n-1 degree polynomial equations. The answer of the equations is the bridge deflection. This method is only applicable to small and single-span bridges. In case of long-span continue beam bridges, it still needs to deploy numbers of expensive and high-precise inclinometers. Moreover, the double integration method(DIM) can also achieve bending deflection curve of an Euler–Bernoulli beam by double integrating strain distribution and the cost of distributed strain sensors are obviously lower than that of high-precise inclinometers. Results from model tests of simple-supported beam show that the maximum difference between the monitoring displacement and the true value is only about 3% [10~12]. Nevertheless, according to the data from a practical deflection monitoring on a multi-span beam bridge, the monitoring error in the second span can rise to over 15%, which is clearly higher than the difference about 3% in the first span[13,14], because measurement errors accumulate in double integrating process. In order to solve this problem, an improved conjugated beam method(ICBM) has been proposed to deduce the influence of error accumulation[15].

Though the mentioned methods for deflection monitoring are suitable for solid rectangular beam suffering bending moment, the applicability may be challenged in case of box girder seen as a kind of typical hollow beam widely employed in long-span bridges because of two remarkable additional deformations caused by shear lag effect and shearing action. For one thing, similar results from different researches [16-18] illustrate that the first additional deformation (AD1) caused by shear lag effect at the mid-span of a simply supported box girder can easily approach 10% of the bending deflection when the height/span ratio exceeds 0.1. For another, the second additional deformation (AD2) caused by shear action can also reach 10% of the bending deflection when the shear span-depth ratio is lower than 1/20[19]. In brief, the existing methods based on the distributed stain measurements, including DIM or ICBM, have to be revised to obtain AD1 or AD2 owing to the differences between the box girder and the Euler–Bernoulli beam.

Moreover, there is another significant argument of obtaining enough strain data by installing minimized quantity of strain sensors to cover the entire box gilder. For this problem, long-gage fiber bragg grating strain sensor [20,21] is proved to be an acceptable solution. The most notable advantage of this sensor is that it can achieve the average strain of a long distance which can reach 0.1m to 10m. It implies that the entire beam can be covered by a few of these sensors. Based on the concept of long-gage strain sensor, a packaged design of LFBG sensor [22] and sensitivity-improved LFBG sensor [23] are proposed to catch slight strain variation in practical monitoring. The LFBG sensor is also verified to be applicable to measure not only dynamic strain [24] but also dynamic displacement [25]. Therefore, the LFBG sensor is seen as a useful tool for high-precision strain measurement with relatively low cost.

This paper is organized as follows. Section 2 introduces the ICBM proposed in our previous research and the LFBG strain sensor used in the experiment in Section 5. Section 3 revises ICBM to monitor AD1 and AD2 based on long-gage strain measuring. Section 4 gives the best position for the LFBG sensor placement. At last, experiments using numerical models and a concrete reduce-scale box girder monitored by LFBG sensors are shown Section 5 to evaluate the theoretical and actual precision of the revised ICBM.

2. ICBM and LFBG sensor

2.1. Improved conjugated beam method

Based on the long-gage strains, ICBM [15] is proposed to provide a linear and explicit relationship between bending deflection and strain distribution, which can be seen as the most attractive benefit rather than DIM which can only give an implicit and double-integrated function.

Preprints (www.preprints.org) | NOT PEER-REVIEWED | Posted: 12 June 2018 doi:10.20944/preprints201806.0166.v1

Peer-reviewed version available at *Sensors* **2018**, *18*, 2597; doi:10.3390/s18082597

Therefore in ICBM, it is easy to predict error accumulation from each monitoring parameter. A simply-supported solid beam is shown in Figure 1(a). It has length L and uniform flexural rigidity EI. The beam is uniformly divided into m elements artificially, denoted as E_1~E_m. The height of the beam is h. The average strains at the top surface and the bottom surface of the E_i are $\varepsilon_i^{\mathrm{B}}$ and ω_i^{B} ($1 \le i \le m$), respectively. Superscript B implies that the variable is used under the pure bending.

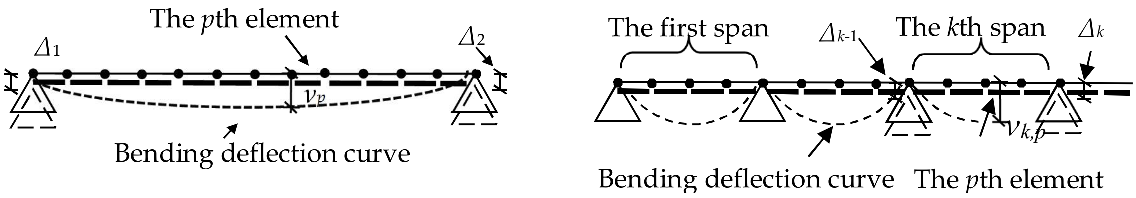

(**a**) a simply-supported beam (**b**) a continue beam

Figure 1. Schematic diagram of a simply-supported solid beam and a continuous multi-spans beam

Without support settlement, the vertical displacement v_p^{B} at the boundary point between E_p and E_{p+1} is:

$$v_p^{\mathrm{B}} = -\frac{L^2}{m^2}\left[\frac{p}{m}\sum_{i=1}^{m}\bar{\kappa}_i^{\mathrm{B}}\left(m-i+\frac{1}{2}\right)-\sum_{i=1}^{p}\bar{\kappa}_i^{\mathrm{B}}\left(p-i+\frac{1}{2}\right)\right] \tag{1}$$

where $\bar{\kappa}_i^{\mathrm{B}}$ is the average curvature of E_i ,which can be calculated by Equation(2). Tensile strain and upward deflection are defined to be positive in this paper.

$$\bar{\kappa}_i^{\mathrm{B}} = \frac{\bar{\omega}_i^{\mathrm{B}} - \bar{\varepsilon}_i^{\mathrm{B}}}{h} \tag{2}$$

Considering combined action of arbitrary loads and support settlements, the vertical displacement v_p^{B} can be revised as follows:

$$v_p^{\mathrm{B}} = -\frac{L^2}{m^2}\left[\frac{p}{m}\sum_{i=1}^{m}\bar{\kappa}_i^{\mathrm{B}}\left(m-i+\frac{1}{2}\right)-\sum_{i=1}^{p}\bar{\kappa}_i^{\mathrm{B}}\left(p-i+\frac{1}{2}\right)\right]+\frac{m-p}{m}\Delta_0+\frac{p}{m}\Delta_1 \tag{3}$$

where Δ_0 and Δ_1 are two support settlements respectively, which can be measured by displacement meters.

ICBM is also adaptive to monitor bending deflection in multi-span bridge shown in Figure 1(b). Δ_{k-1} and Δ_k represent settlements occurred at two supports of the kth span of this bridge. The kth span is equally divided into n elements named as $E_{k,1}$~$E_{k,n}$. The length and the height of the kth span are L_k and h_k, respectively. The average strains at the top surface and the bottom surface of the $E_{k,i}$ are $\bar{\varepsilon}_{k,i}^{\mathrm{B}}$ and $\bar{\omega}_{k,i}^{\mathrm{B}}$ ($1 \le i \le m$), respectively. So the vertical displacement $v_{k,p}^{\mathrm{B}}$ at the boundary point between $E_{k,p}$ and $E_{k,p+1}$ in the kth span is:

$$v_{k,p}^{\mathrm{B}} = -\frac{L_k^2}{m^2}\left[\frac{p}{m}\sum_{i=1}^{m}\bar{\kappa}_{k,i}^{\mathrm{B}}\left(n-i+\frac{1}{2}\right)-\sum_{i=1}^{p}\bar{\kappa}_{k,i}^{\mathrm{B}}\left(p-i+\frac{1}{2}\right)\right]+\frac{m-p}{m}\Delta_{k-1}+\frac{p}{m}\Delta_k \tag{4}$$

where $\bar{\kappa}_{k,i}^{\mathrm{B}}$ is the average curvature of $E_{k,i}$,which can be calculated by Equation (5).

$$\bar{\kappa}_{k,i}^{\mathrm{B}} = \frac{\bar{\omega}_{k,i}^{\mathrm{B}} - \bar{\varepsilon}_{k,i}^{\mathrm{B}}}{h_k} \tag{5}$$

From Equation (1) to Equation (5), two remarkable features of ICBM can be summarized as follows:

I. The formula of ICBM is linear and explicit. All parameters are free from actual load patterns or flexural rigidity of the monitored beam.
II. Precision of bending deflection monitoring in one span is just related to the measurement errors of strain distribution in the same span. It implies that measurement error accumulation of one span cannot affect monitoring results of bending deflection in other spans.

Moreover, it is noted that the ICBM is effective on a basic assumption of "solid beam". It represents that the beam has enough rigidity to keep a changeless shape regardless of loading mode (LM). However, when minor change occurs on the cross-section shape of box girder under the action of LM changing, ICBM needs to be updated again.

Preprints (www.preprints.org) | NOT PEER-REVIEWED | Posted: 12 June 2018 doi:10.20944/preprints201806.0166.v1
Peer-reviewed version available at Sensors 2018, 18, 2597; doi:10.3390/s18082597

2.2. LFBG strain sensor

In concrete structures, precise and long-term strain monitoring is quite difficult due to concrete crack. Figure 2 gives a comprehensive illustration to show the traditional strain measuring by short-gage sensors (Sensor A and Sensor B) which are entirely bonded on the surface of the structure with resin. Before concrete cracking, both of them catch the true concrete strain. Nevertheless, after crack occurring, Sensor A is over sketched to snap because its gauge just covers the crack. And strain in Sensor B is almost released at the same time. It is obvious that the measurements from such short-gage sensor cannot represent the true strain increasing. Compared with short-gage sensor, long-gage sensor has aroused increasing concern for its point fixation, which implies that only two ends of the sensor are bonded to the specimen to form a uniform strain distribution in its gauge. The most notable advantage of long-gage sensor is the fact that the sensor can avoid sudden rupture induced by concrete crack because the sensing part in the sensor has a little distance away from the concrete surface. Therefore, it is found that long-gage sensor has more applicability than traditional short-gage sensor in strain monitoring for concrete structures.

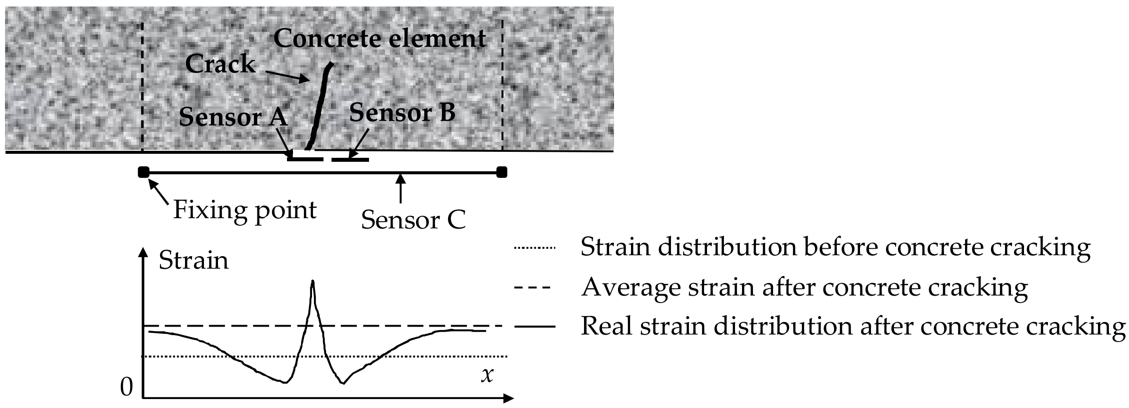

Figure 2. Different strain measurements from three sensors before and after concrete cracking

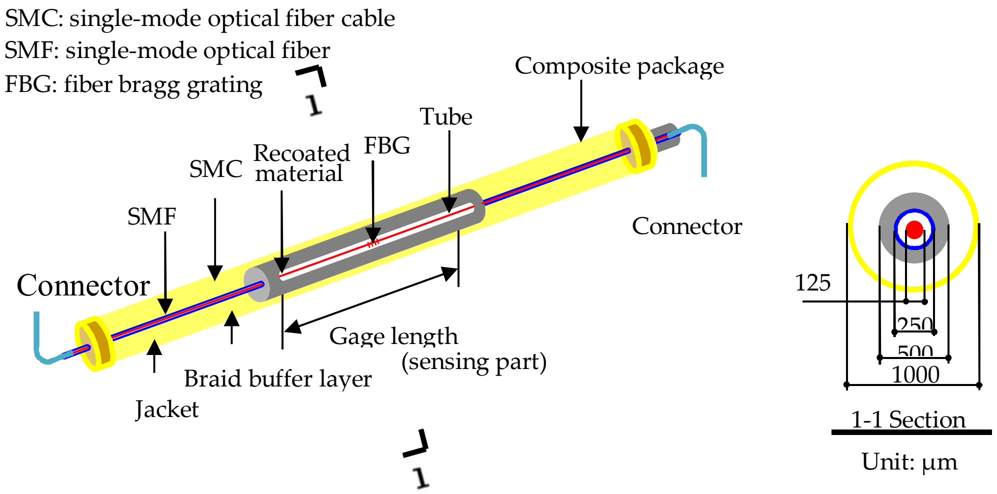

Figure 3. Structural design of packaged LFBG sensor [22]

On the other hand, it can obviously save monitoring and maintenance cost if all sensor can constitute a sensing network to share the same signal source, connecting wire and demodulation system. Fiber Bragg Grating (FBG) sensor, which is characterized by distributed sensing along a single optical fiber, exactly meets the mentioned requirements. Based on FBG sensor, Li [22] proposed Long-gage Fiber Bragg Grating (LFBG) sensor which successfully interweaves the precision and distributed sensing characteristic of FBG sensor and the applicability of long-gage

 doi:10.20944/preprints201806.0166.v1

Peer-reviewed version available at *Sensors* **2018**, *18*, 2597; doi:10.3390/s18082597

sensor in long-term strain monitoring. Considering these benefits, LFBGS shown in Figure 3 is used in this paper to measure long-gage strain in each element of box girder.

3. Theoretical improvement for ICBM to monitor AD1 and AD2 in a single-cell box girder

Results from theoretical derivation and numerical simulation indicate that the total deformation of a box girder can be devoted to three parts – bending deflection which is the main portion in the total deformation, AD1 caused by shear lag effect and AD2 caused by shear action. Considering bending deflection can be obtained by ICBM, this part derives the relationship between AD1, Ad2 and distributed long-gage strain measurement. The deriving process is based on the following assumptions. First, material used is isotropic and elastic. Second, the stress-strain curve of material used is linear. Third, shear lag effect can only affect stress distribution on cross-section and it cannot influence stress distribution in the longitudinal direction. Fourth, total deformation of the single-cell box girder is still relatively small. At last, torsion, torsional warping and distortion are ignored in the derivation of this paper.

3.1. AD1 calculating based on strain distribution

Shear lag effect represents a phenomenon on cross-section of box girder that the longitudinal stress on a flange near the web is much larger than that far from the web. Obviously, it is quite different from the uniform stresses distribution assumption in the elementary beam theory. This phenomenon also implies that the flange far from the web on the cross-section is barely contributed to flexural rigidity. Therefore, an additional curvature occurs on of the section due to the extra decrease in flexural rigidity calculated according to the elementary beam theory. AD1 is the macroscopic result from accumulation of additional curvature.

Results from numerical simulations [17] point out that the practical curvature of the section equals to the product of λ and curvature calculated according to the elementary beam theory, where λ is shear lag coefficient defined as the ratio of the normal stresses to those obtained according to the elementary beam theory. This conclusion has two meanings. One is that AD1 is a special bending deflection essentially and the equation (1) is applicable to describe the relationship between AD1 and the additional curvature increments in all elements. The other is that the actually measured average strains are also the products of λ and strains calculated according to the elementary beam theory, which is shown as $\bar{\beta}_i$ ($\bar{\beta}_i=\lambda_i\bar{\varepsilon}_i^{\mathrm{B}}$) and $\bar{\alpha}_i$ ($\bar{\alpha}_i=\lambda_i\bar{\omega}_i^{\mathrm{B}}$). Therefore, the curvature $\bar{\kappa}_i^{\mathrm{B}}$ in Equation (2) has to be replaced by $\bar{\gamma}_i$ ($\bar{\gamma}_i=\lambda_i\bar{\kappa}_i^{\mathrm{B}}$), where λ_i is shear lag coefficient of E_i. Superscript SL implies that the variable is used under shear lag action. Then this expression of $\bar{\gamma}_i$ is shown as follows:

$$\bar{\gamma}_i=\lambda_i\bar{\kappa}_i^{\mathrm{B}}=\bar{\kappa}_i^{\mathrm{B}}+\bar{\kappa}_i^{\mathrm{SL}}=\bar{\kappa}_i^{\mathrm{B}}+(\lambda_i-1)\bar{\kappa}_i^{\mathrm{B}}=\frac{\bar{\omega}_i^{\mathrm{B}}-\bar{\varepsilon}_i^{\mathrm{B}}}{h}+(\lambda_i-1)\frac{\bar{\omega}_i^{\mathrm{B}}-\bar{\varepsilon}_i^{\mathrm{B}}}{h}=\frac{\lambda_i\bar{\omega}_i^{\mathrm{B}}-\lambda_i\bar{\varepsilon}_i^{\mathrm{B}}}{h}=\frac{\bar{\alpha}_i-\bar{\beta}_i}{h} \tag{6}$$

As a result, the AD1 represented as v_p^{SL} at the boundary point between E_p and E_{p+1} is:

$$\begin{aligned}
v_p^{\mathrm{SL}}&=-\frac{L^2}{m^2}\left[\frac{p}{m}\sum_{i=1}^{m}\bar{\kappa}_i^{\mathrm{SL}}\left(m-i+\frac{1}{2}\right)-\sum_{i=1}^{p}\bar{\kappa}_i^{\mathrm{SL}}\left(p-i+\frac{1}{2}\right)\right]\\
&=-\frac{L^2}{m^2}\left[\frac{p}{m}\sum_{i=1}^{m}(\lambda_i-1)\bar{\kappa}_i^{\mathrm{B}}\left(m-i+\frac{1}{2}\right)-\sum_{i=1}^{p}(\lambda_i-1)\bar{\kappa}_i^{\mathrm{B}}\left(p-i+\frac{1}{2}\right)\right]\\
&=-\frac{L^2}{m^2}\left[\frac{p}{m}\sum_{i=1}^{m}\lambda_i\bar{\kappa}_i^{\mathrm{B}}\left(m-i+\frac{1}{2}\right)-\sum_{i=1}^{p}\lambda_i\bar{\kappa}_i^{\mathrm{B}}\left(p-i+\frac{1}{2}\right)\right]+\frac{L^2}{m^2}\left[\frac{p}{m}\sum_{i=1}^{m}\bar{\kappa}_i^{\mathrm{B}}\left(m-i+\frac{1}{2}\right)-\sum_{i=1}^{p}\bar{\kappa}_i^{\mathrm{B}}\left(p-i+\frac{1}{2}\right)\right]\\
&=-\frac{L^2}{m^2}\left[\frac{p}{m}\sum_{i=1}^{m}\bar{\gamma}_i\left(m-i+\frac{1}{2}\right)-\sum_{i=1}^{p}\bar{\gamma}_i\left(p-i+\frac{1}{2}\right)\right]-v_p^{\mathrm{B}}
\end{aligned} \tag{7}$$

Consequently, the sum of v_p^{B} and v_p^{SL} is given by following:

$$v_p^{\mathrm{B}}+v_p^{\mathrm{SL}}=-\frac{L^2}{m^2}\left[\frac{p}{m}\sum_{i=1}^{m}\bar{\gamma}_i\left(m-i+\frac{1}{2}\right)-\bar{\gamma}_i\left(p-i+\frac{1}{2}\right)\right] \tag{8}$$

Considering combined action of arbitrary loads and support settlements, the sum of v_p^{B} and v_p^{SL} is revised as follows:

Preprints (www.preprints.org) | NOT PEER-REVIEWED | Posted: 12 June 2018 doi:10.20944/preprints201806.0166.v1

Peer-reviewed version available at Sensors 2018, 18, 2597; doi:10.3390/s18082597

$$v_p^{\mathrm{B}} + v_p^{\mathrm{SL}} = -\frac{L^2}{m^2}\left[\frac{p}{m}\sum_{i=1}^{m}\overline{\gamma}_i\left(m-i+\frac{1}{2}\right) - \sum_{i=1}^{p}\overline{\gamma}_i\left(p-i+\frac{1}{2}\right)\right] + \frac{(m-p)}{m}\Delta_0 + \frac{p}{m}\Delta_1 \tag{9}$$

3.2. AD2 calculating based on strain distribution

Before the deriving process of AD2's expression, it is worth discussing a relative problem which is whether shear action brings extra longitudinal strain. It is proposed in the material mechanics that the extra longitudinal strain can be ignored in a slender beam subjected to a uniformly distributed load. When the beam is subjected to a concentrated load, the influence in strain from shear action is still approximate to zero except for the area near to the supporting points. Therefore, it is conclude that the longitudinal strain is free from shear action in the deriving process of AD2's expression.

Timoshenko [26] points out that the first derivative of $v^S(x)$ with respect to x equals to the shear strain in neutral axis of cross-section. Superscript S implies that the variable is used under shear action. This point can be expressed as follows:

$$\frac{dv^{\mathrm{S}}(x)}{dx} = -\frac{\eta V(x)}{AG} \tag{10}$$

where x is the longitudinal coordinate. G and A are shear modulus of material and cross-section area, respectively. $V(x)$ is shear force along the section. η is shear correction factor which equals to the ratio of shear stress τ_{NA} on neutral axis to average shear stress $\overline{\tau}$ on the entire section.

Because shear force $V(x)$ is the first derivative of moment $M(x)$, Equation (10) can be transformed into:

$$\frac{dv^{\mathrm{S}}(x)}{dx} = -\frac{\eta}{AG}\frac{dM(x)}{dx} \tag{11}$$

Integrating on both sides of Equation (11) from 0 to x and considering both $v^S(0)$ and $M(0)$ equal to 0 in case of simply-supported condition, it is obtained as follows:

$$v^{\mathrm{S}}(x) = -\frac{\eta}{AG}M(x) \tag{12}$$

Shear correction factor η can be expressed by following:

$$\eta = \frac{\tau_{\mathrm{NA}}}{\overline{\tau}} = \frac{VS_y}{2t_{\mathrm{NA}}I\overline{\tau}} = \frac{AS_y}{2t_{\mathrm{NA}}I} \tag{13}$$

where S_y is the first moment with respect to the neutral axis of the area on one side of the neutral axis. V and I respectively represent shear force on neutral axis and moment of inertia of the entire cross-sectional area. t_{NA} is width of web, which is measured on the same height of neutral axis.

Substituting Equation (13) into Equation (12), Equation (12) can be simplified as follows:

$$v^{\mathrm{S}}(x) = -\frac{S_y}{2Gt_{\mathrm{NA}}I}\cdot M(x) = -\frac{(1+\mu)S_y}{t_{\mathrm{NA}}}\cdot\frac{M(x)}{EI} = -\frac{(1+\mu)S_y}{t_{\mathrm{NA}}}\cdot\kappa^{\mathrm{B}}(x) = -\frac{(1+\mu)S_y}{\lambda t_{\mathrm{NA}}}\cdot\gamma(x) \tag{14}$$

where E and μ respectively represent the elastic module and Poisson's ratio of material.

Therefore, the AD2 named as v_p^{S} at the boundary point between E_p and E_{p+1} is:

$$v_p^{\mathrm{S}} = -\frac{(1+\mu)S_y}{(\lambda_p+\lambda_{p+1})t_{\mathrm{NA}}}\cdot(\overline{\gamma}_p+\overline{\gamma}_{p+1}) \tag{15}$$

It is noted that the shear lag coefficient λ of each element is predetermined before calculating Equation (13). However, the value of λ fluctuates according to different LMs and different positions. Besides, it is difficult to identify the accurate LM in the real structure in practical monitoring. As a result, keeping a constant value for λ in entire calculating process is a simple and feasible solution. On the basis of references [16,27], Table 1 gives recommended value of λ for a single-cell beam under simply-supported condition.

Table 1. Recommended value of λ for a single-cell beam under simply-supported condition [27]

L/b^1	6	8	≥10
λ	1.22	1.15	1.10

[1] L and b are the entire length of the beam and the width of flange, respectively.

So Equation (13) can be simplified as follows:

$$v_p^{\mathrm{S}} = -\frac{(1+\mu)S_y}{2\lambda t_{\mathrm{NA}}}\cdot(\bar{\gamma}_p+\bar{\gamma}_{p+1}) \tag{16}$$

Finally, the entire deformation v including bending deflection, AD1 and AD2 are obtained by following:

$$v = v_p^{\mathrm{B}} + v_p^{\mathrm{SL}} + v_p^{\mathrm{S}} = -\frac{L^2}{m^2}\left[\frac{p}{m}\sum_{i=1}^{m}\bar{\gamma}_i\left(m-i+\frac{1}{2}\right)-\sum_{i=1}^{p}\bar{\gamma}_i\left(p-i+\frac{1}{2}\right)\right]-\frac{(1+\mu)S_y}{2\lambda t_{\mathrm{NA}}}\cdot(\bar{\gamma}_p+\bar{\gamma}_{p+1})+\frac{(m-p)}{m}\Delta_0+\frac{p}{m}\Delta_1 \tag{17}$$

4. The best choice for LFBG sensor placement

As shown in Figure 4(a), strain distribution on the flange of a box girder is nonuniform due to action of shear lag effect. It illustrates that strain sensor placement in the box girder deserve to be deliberately discussed. As illustrated in Figure 4(b), there are five possible locations from A to E for placement of LFBG sensor. Nevertheless, two preconditions are worth considering. The first one is that fixing sensor on the outer surface of a box girder is usually more available than that on the inner surface of a box girder. The other one is that the strain distribution around the practical fixing location needs to follow the plane-section assumption and to be far from influence of shear lag. According to the two preconditions, it is obvious that C+D may be the most suitable choice for the LFBG sensor placement in practice.

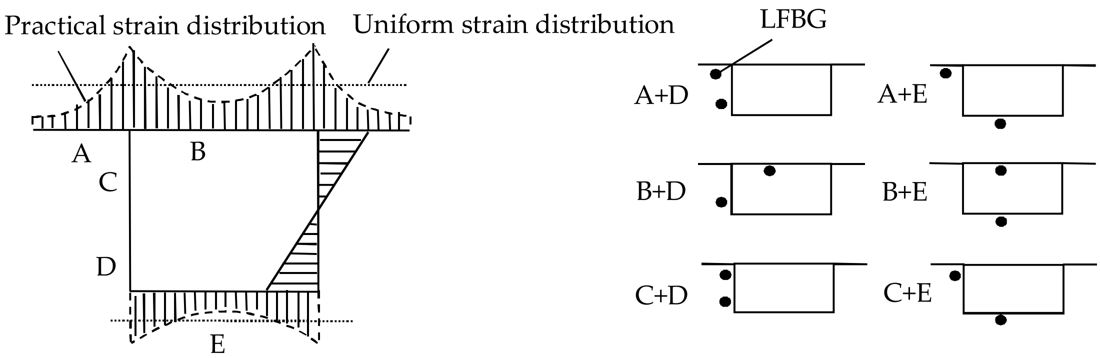

(**a**) Strain distribution on section (**b**) 6 schemes of sensor placement

Figure 4. Several schemes of sensor placement base on strain distribution

5. Verification of revised ICBM: Numerical simulation

There are two types of errors which can decrease the accuracy of monitored deformation. One is algorithm error from inaccuracy of simulation for real structures, and the other is measuring error in practical strain monitoring. In this verification, a numerical model simulating a real single-cell box girder under different loading modes (LMs) is used to evaluate the influence of algorithm error from revised ICBM. Evaluation for effect of measuring error accumulation in experimental test is carried out in the next part.

5.1. Detailed design for the numerial model, sensor placement and loading mode

The numerical model is built based on the solid45 element in ANSYS software. Details about a single-cell concrete box gilder with single-supported boundary condition are illustrated in Figure 5. The dimensions of the cross-section are as follows: b=400mm, t_u=t_w=t_b=t_{NA}=50mm, h=300mm, L=3600mm. The compressive strength of concrete is 23.1N/mm^2. The elastic module and Poisson's ratio of concrete are 34.5GPa and 0.2, respectively. This beam is uniformly divided into 18 elements, denoted as E_1~E_{18}.

There are three different LMs applied to the model, which are uniform loading, loading at midpoint and loading at trisection points, respectively. According to Table 1, λ is 1.1 due to

doi:10.20944/preprints201806.0166.v1

Peer-reviewed version available at *Sensors* **2018**, *18*, 2597; doi:10.3390/s18082597

L/b=3600/400=9. Surface load q is 20kN/m². Linear loads include f_0, f_1 and f_2 , whose values are 41.25 kN/m, 41.25 kN/m and 20.625 kN/m, respectively.

A series of long-gage strain sensors are simulated to fixed at the two horizontal edges of each element in the web. The distance d between the upper part and lower part of sensors is 250mm.

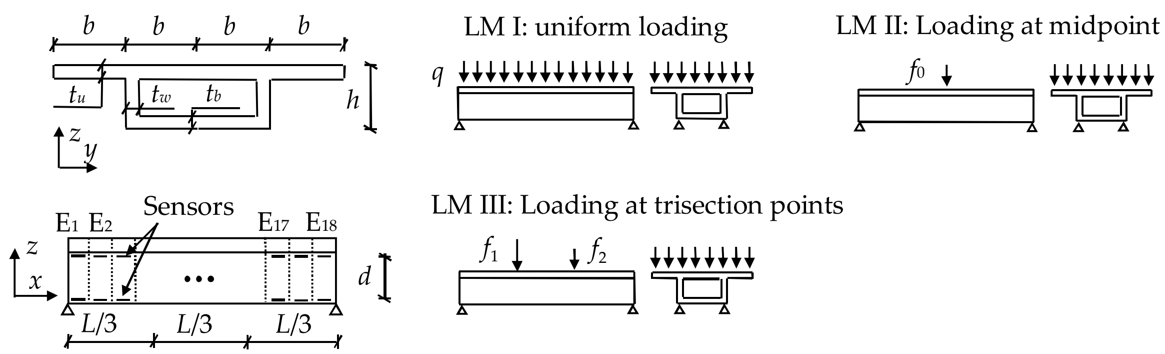

Figure 5. Detailed design for the numerical model of a single-cell box gilder in 3 different LMs

5.2. Results and Analysis

Long-gage strain measurements of 18 elements in different LMs are given in Table 2. It is noted that in each element, compressive strain occurs in upper part and tensile strain occurs in lower part. Figure 6 gives the distances between the neutral axis and the bottom surface of each element in 3 different LMs. Calculation formula is given in Equation (18). It is clear that the height of neutral axises of E3~E16 keep almost in the range of 152mm~153mm except for small variation occurring in some elements near concentrated loads such as E9, E10 in LM II and E6, E7, E12, E13 in LM III. Due to boundary restraints, tensile strains of E1 and E18 are larger than those of other elements. This leads to the result that the height of neutral axises of E1, E2, E17 and E18 are obvious larger than those of other elements. Therefore, the partial and small variation about height of neutral axises shows the approximate application of the plane-section assumption in web.

$$\text{Distance in each element} = \frac{\bar{\alpha}_i / \bar{\beta}_i}{1 + \bar{\alpha}_i / \bar{\beta}_i} \cdot d \tag{18}$$

Table 2. Long-gage strains at the top and bottom of each element on the finite element model of the box girder (Unit: με)

LM		E1	E2	E3	E4	E5	E6	E7	E8	E9	E10	E11	E12	E13	E14	E15	E16	E17	E18
1	$\bar{\beta}_i$	-5	-35	-57	-69	-80	-89	-96	-101	-103	-103	-101	-96	-89	-80	-69	-57	-35	-5
	$\bar{\alpha}_i$	128	83	88	108	126	141	153	160	164	164	160	153	141	126	108	88	83	130
2	$\bar{\beta}_i$	2	-18	-33	-44	-55	-68	-83	-101	-130	-130	-101	-83	-68	-55	-44	-33	-18	2
	$\bar{\alpha}_i$	71	46	53	71	90	110	134	165	195	195	165	134	110	90	71	53	46	73
3	$\bar{\beta}_i$	2	-31	-56	-77	-101	-139	-147	-125	-116	-110	-108	-113	-103	-78	-60	-44	-24	2
	$\bar{\alpha}_i$	119	77	89	123	165	208	221	204	187	179	177	175	159	128	97	71	61	97

Preprints (www.preprints.org) | NOT PEER-REVIEWED | Posted: 12 June 2018 doi:10.20944/preprints201806.0166.v1

Peer-reviewed version available at *Sensors* **2018**, *18*, 2597; doi:10.3390/s18082597

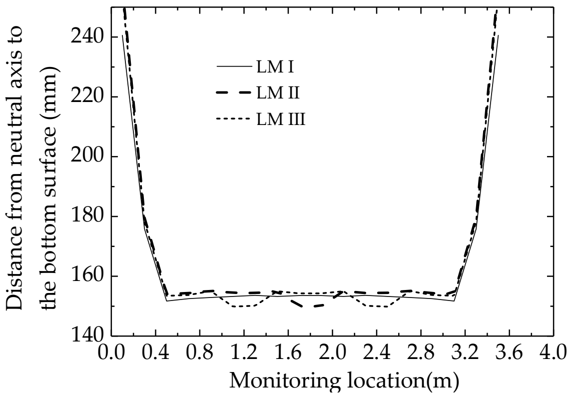

Figure 6. Distance from the neutral axis to the bottom surface of each element in different LMs

A comparison is made between monitored deformations and true deformations under the different LMs, which are shown in Figure 7(a)~(c). The dash lines and the solid lines respectively represent the true deformations and the monitored deformations calculated by substituting strain data in Table 2 to Equation 17 (λ=1.1). The dot dash lines and the dot lines in Figure 7 are AD2 and sum of AD1 and AD2, respectively. It is found that either AD1 or AD2 accounts for about 10% of the total deformations. These proportions illustrate that neither of AD1 or AD2 can be ignored in this model. Moreover, most of deviations between monitored deformations and true deformations are about 0.3%~1.5% except those of E9, E10 in LM II which are 2.4%. In fact, the accurate value of λ under the condition of uniform loading is about 1.069~1.079, which is quite close to the constant value of 1.10. The accurate value of λ in E9, E10 under the condition of concentrated loading is 1.266, which is larger than 1.10. This deviation may be the main reason leading to the error of 2.5% in calculated deformation of E9, E10 in LM II.

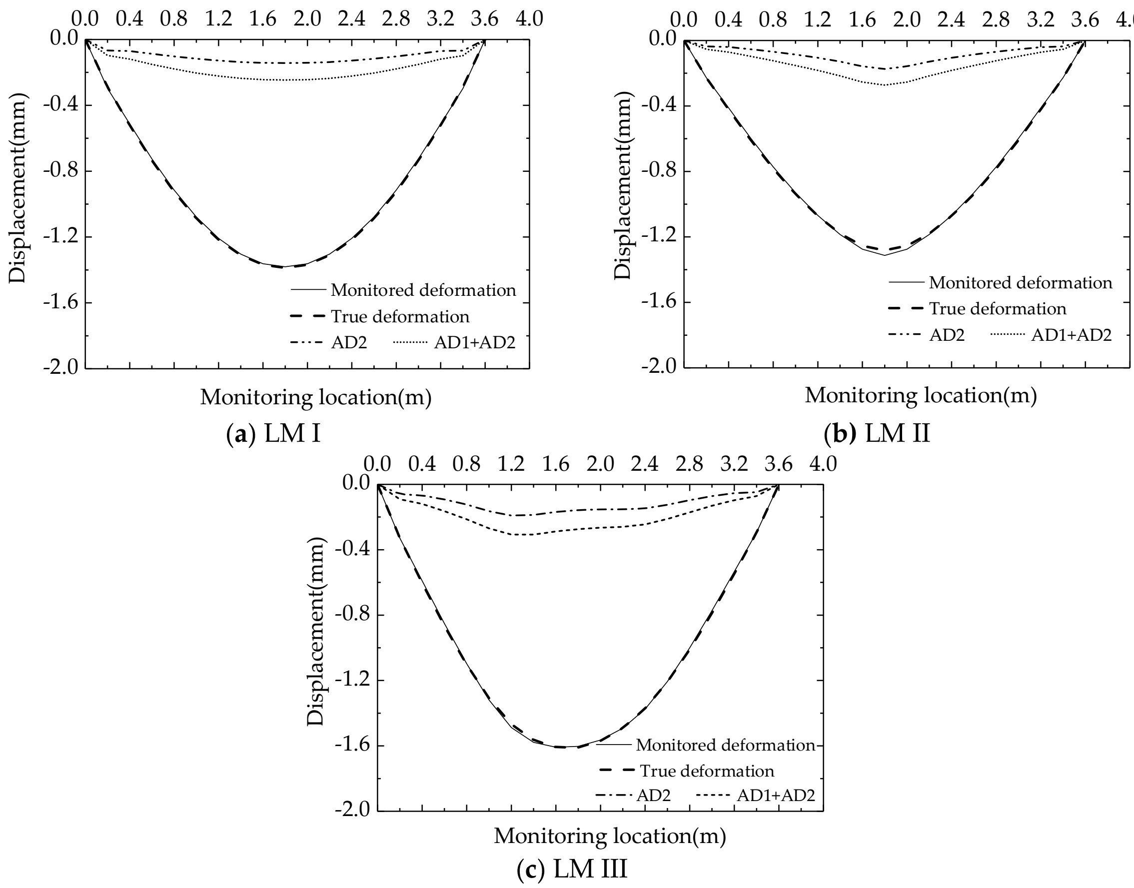

Figure 7. Comparison between monitored deformations and true deformations in case of different LMs

Preprints (www.preprints.org) | NOT PEER-REVIEWED | Posted: 12 June 2018 doi:10.20944/preprints201806.0166.v1

Peer-reviewed version available at *Sensors* **2018**, *18*, 2597; doi:10.3390/s18082597

Table 3 gives monitoring errors between monitoring displacements and true displacements in 1/3 span, mid span and 2/3 span. It is evident that the monitoring errors may slightly reduce if λ is substituted to its accurate value. The maximum error decreases from 2.4% to 0.6% at the mid span in LM II. Because the LM in actual bridge is usually difficult to measure, it is an applicable solution to give a constant value to λ in the calculating process with little influence to the precision of deformation monitoring for a single-cell box gilder.

Table 3 Monitoring errors between monitored displacements and true displacements in three positions (unit :%)

LM	Value of λ	Positions		
		1/3 span	Mid span	2/3 span
I	λ=1.1	-0.6	-0.4	-0.6
	λ=accurate value	-0.5	-0.1	-0.5
II	λ=1.1	-0.3	2.4	-0.3
	λ=accurate value	0.5	0.6	0.5
III	λ=1.1	1.5	-0.3	0.3
	λ=accurate value	0.3	0.4	-0.6

6. Verification of revised ICBM: Experiment

This experiment has two main purposes. One is to show the effectiveness of revised ICBM to obtain accurate deformation in actual single-cell concrete box girder. The other is to investigate the possibility of replacing the true λ with a constant value in practical calculating process.

6.1 Test Setup and Sensor Placement

Details regarding the beam dimensions and reinforcement configuration of a simply-supported single-cell box girder are illustrated in Figure 8. It can be found that the dimensions of the section and the entire length of the beam are as same as the simulated model shown in Figure 5. The compressive strength of concrete is about 39N/mm^2. The elastic modulus and Poisson's ratio of concrete are 3.03×10^4 N/mm^2 and 0.19, respectively. In Figure 8, 20 reinforcements 6 mm in diameter and 11 passive reinforcements 12 mm in diameter are used for longitudinal bars, located 20 mm away from the edges of the beam. There are also 2 passive reinforcements 6 mm in diameter in each web of the beam. Stirrups are deployed throughout the entire length of the beam, with 6 mm diameter and 100 mm distance in two adjacent vertical bars. The yield strength of the bars is about 380N/mm^2. All mentioned material parameters are determinate by standard experiments. Moreover, there are four steel baffles placed at two trisection points and two ends of the beam to prevent torsional warping and distortion.

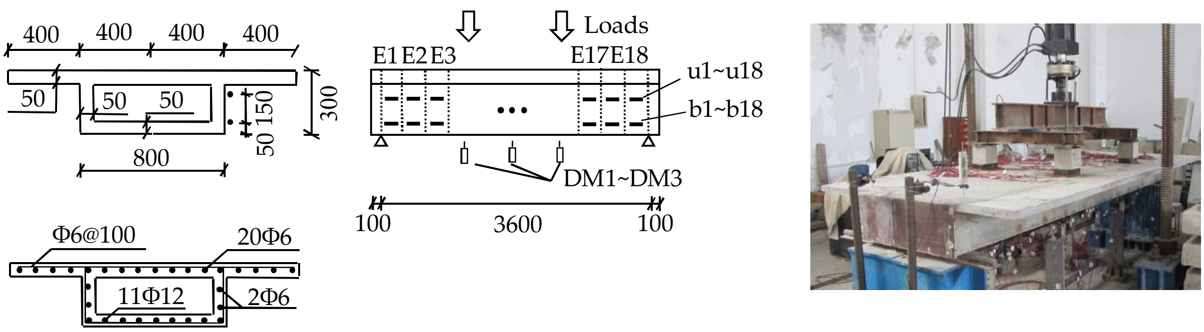

(a) Design for the sing-cell box gilder with sensors placement (b)Photograph of experiment

Figure 8. Outline of the sing-cell box gilder and the experiment (unit: mm)

The single-cell box gilder is artificially divided into 18 zones with a uniform length of 200 mm, as denoted by Element1~Element18 (E1~E18). 36 LFBG sensors with a uniform length of 180mm are installed on the surface of one web of the beam. Half of LFBG sensors named as b1~b18 are fixed at the position 50mm higher than the bottom of beam. By contrast, the other half named as u1~u18 are fixed at the position 200mm higher than the bottom of beam. Obviously, it has a distance of 150mm between the two parts of sensors. Three displacement meters (DM1~DM3) are installed at the two trisection points (point A, point C) and the midpoint B of the beam. Point A, B and C are the boundary points between E6 and E7, E9 and E10, E12 and E13, respectively.

The load is divided equivalently into two parts by using a transferred steel board landing at two points 1200 mm from each support. The increasing load is continuously applied by 5 successive loading steps (LSs) from 0 to 10KN, 15KN, 20KN, 25KN and 30KN. The maximum measured strain is ensured to be lower than 100με considered as the ultimate tensile strain of concrete. All strain measurements are revised by temperature compensation.

6.2. Results and Analysis

Table 4 gives the long-gage strain measurements from LFBG sensors placed on the surface of each element in different LSs. It is evident that in each element, the measured strains from b1~b18 are positive, whereas the measured strains from u1~u18 are negative. This trend illustrates that the testing single-cell box girder mainly suffers increasing bending moments as rising loads. The bending moments brings tension to the lower part of the beam and compression to the upper part of the beam. Figure 9(a)~(c) respectively gives the comparisons between the monitored displacements of point A, B and C in different LSs, which are calculated from the strain measurements given in Table 4. Upward deformation is defined to be positive. The symbol ■ means that λ equals to a constant value of 1.1 according to Table 1 during the calculating process. The symbol □ represents that λ equals to the accurate values at corresponding monitoring points. At point A, C and point B, the accurate value of λ is 1.2 and 1.017, respectively. Table 5 shows the comparison of monitoring error percentages between the monitored displacements and the true displacements in each LS. It can be noted that the monitored displacements agree well with the true displacements. Most of the errors range from 6%~8%, and the maximum monitoring error is only 11.0%. This agreement implies the applicability of revised ICBM for deformation monitoring to a single-cell box gilder based on LFBG sensors. In addition, the fact that influence from different values of λ in deformation monitoring is almost lower than 1% shows that λ can be determinate approximately to a constant value according to Table 1 to not only reduce the difficulty of parameter determining but also ensure accuracy of monitored deformations. Moreover, comparison between monitoring errors from Table 3 and Table 5 shows that the precision of monitored deformations is depended on the precision of sensors rather than algorithm error. It illustrates the importance of long-term monitoring precision and durability of long-gage sensors in practical deformation monitoring.

Table 4 Average strain measurements at the bottom and the top of each element (Unit: με)

		E1	E2	E3	E4	E5	E6	E7	E8	E9	E10	E11	E12	E13	E14	E15	E16	E17	E18
1	$\bar{\beta}_i$[1]	-2	-2	-2	-3	-5	-2	-3	-6	-5	-6	-3	-2	-5	-3	-2	-2	-3	1
	$\bar{\alpha}_i$	1	3	5	7	10	13	14	13	12	11	13	15	13	11	7	6	3	2
2	$\bar{\beta}_i$	-2	-2	-4	-5	-6	-4	-5	-8	-7	-7	-8	-5	-4	-5	-6	-4	-2	0
	$\bar{\alpha}_i$	1	2	7	11	15	18	20	19	18	17	19	21	19	13	12	7	2	0
3	$\bar{\beta}_i$	-3	-3	-5	-7	-9	-6	-7	-11	-10	-10	-11	-7	-9	-8	-4	-3	-2	-2
	$\bar{\alpha}_i$	2	5	10	14	19	24	26	25	24	25	24	26	24	19	15	9	6	1
4	$\bar{\beta}_i$	-4	-4	-6	-8	-7	-8	-9	-15	-9	-12	-12	-14	-9	-10	-8	-6	-4	-2
	$\bar{\alpha}_i$	4	7	11	21	20	33	35	33	27	33	34	35	28	30	22	10	9	5
5	$\bar{\beta}_i$	-4	-5	-7	-9	-7	-9	-10	-17	-10	-15	-16	-9	-9	-13	-9	-7	-5	-2
	$\bar{\alpha}_i$	6	8	15	22	27	37	40	33	34	38	39	45	36	30	22	15	8	5

[1] $\bar{\alpha}_i$ and $\bar{\beta}_i$ are the practical strain measurements from LFBG bi and LFBG ui (i=1~18) , respectively.

 doi:10.20944/preprints201806.0166.v1

Peer-reviewed version available at *Sensors* **2018**, *18*, 2597; doi:10.3390/s18082597

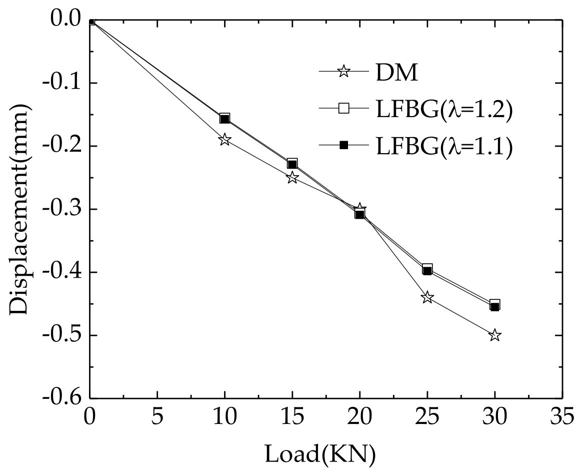

(**a**) LM I

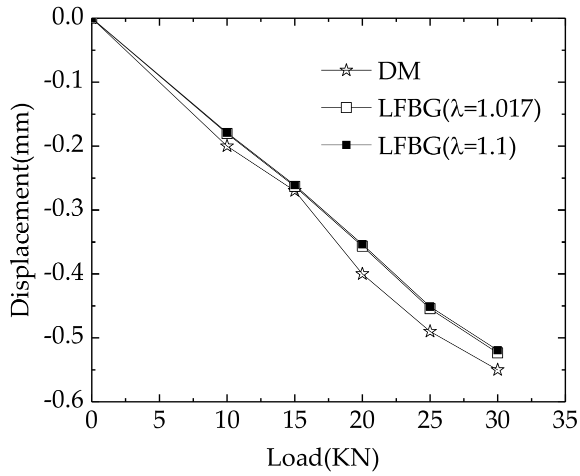

(**b**) LM II

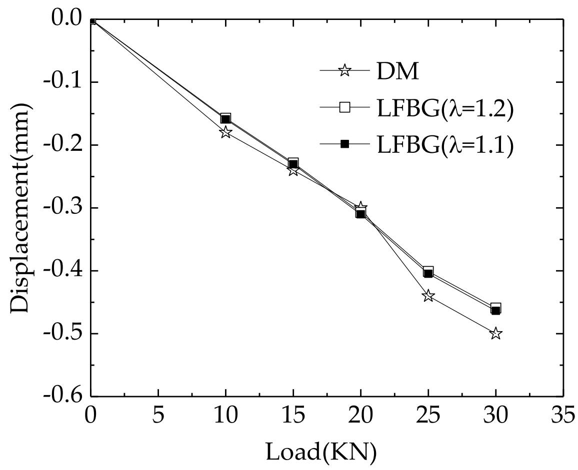

(**c**) LM III

Figure 9. Comparison between monitored displacements and true displacements in case of different LMs

Table 5 Monitoring errors between monitored displacements and true displacements in different points (unit :%)

Loading step		1	2	3	4	5
Point A	λ=1.1	-10.2	-8.2	-6.4	-9.5	-9.0
	λ=1.2	-11.0	-9.1	-7.2	-10.4	-9.8
Point B	λ=1.1	-10.5	-3.3	-11.6	-7.9	-5.6
	λ=1.017	-9.8	-2.5	-10.9	-7.2	-4.8
Point C	λ=1.1	-9.1	-3.9	-6.0	-8.0	-7.3
	λ=1.2	-10.0	-4.8	-6.9	-8.9	-8.2

7. Conclusions

Based on the previous researches about ICBM used to monitor the deformation of solid beam, a revised ICBM is proposed in this paper to accurately gain the entire deformation of single-cell box gilder with simply-supported boundary condition. The best position for sensor placement is also given for practical monitoring. Verifications using numerical simulations and a reduce-scale box gilder monitored by a series of LFBG sensors are carried out to show the theoretical and practical precision of the revised ICBM. After theoretical and experimental investigation, the following conclusions can be drawn:

(1) For a single-cell box gilder, it is verified that revised ICBM, which can still present a linear and explicit function between the deformation and the long-gage strain distribution, is applicable to monitor the entire deformation which contains the bending deflection, AD1 caused by shear lag and AD2 caused by shear action.

(2) The LFBG sensor seen as a typical long-gage strain sensor is useful to not only achieve the strain distributing on the structural surface but also keep a balance between measurements and cost.

(3)In calculating process, the shear lag coefficient λ can be determinate to a constant value to not only avoid the difficulty of investigating loading mode but also ensure the practical precision of monitored deformation.

(4) Results from numerical simulations show that the most of algorithm errors are about 0.3% to 1.5%, and the maximum error is about 2.4%. Results from testing a single-cell box gilder monitored by a series of LFBG sensors show that most of the practical errors range from 6%~8%, and the maximum error is about 11%. It implies that in practical monitoring, errors in monitored deformation are mainly induced by errors in strain measurements rather than algorithm error from revised ICBM.

Acknowledgments: The work is supported by the Technique Project of Fuzhou (Grant No.2017-G-74), the Education and Scientific Research Project for Young and Middle-aged Teachers of Fujian Province (Grant No. JAT160044), the fund of the Hebei Province Key Laboratory of Evolution and Control of Mechanical Behavior in Traffic Engineering Structure (Shijiazhuang Tiedao University), the Transportation and Communication Science and Technology Project of Fujian Province(Grant No. 201536) and the Major Research Projects of the Hebei Provincial Education Department(Grant No.ZD2015060). Moreover, Mr Ke-ke Xu and Ms Ping Han provide helps in the experiments. The authors would appreciate for their help and the anonymous referees for their constructive comments and suggestions.

Author Contributions: The theoretical derivation and two kinds of verifications are finished by Sheng Shen. The paper is revised and finalized by Shao-fei Jiang.

Conflicts of Interest: The authors declare no conflict of interest.

References

1. Mill, T.; Ellmann, A.; Kiisa, M.; Idnurm, J.; Idnurm, S.; Horemuz, M.; Aavik, A. Geodetic monitoring of bridge deformations occurring during static load testing. *Baltic J. Road Bridge Eng* **2015**, 10(1), 17–27, 10.3846/bjrbe.2015.03
2. Kuzina, E.; Rimshin, V. Deformation monitoring of road transport structures and facilities using engineering and geodetic techniques. *International Scientific Conference Energy Management of Municipal Transportation Facilities and Transport (EMMFT2017)*, Khabarovsk, Russia, 10-13 April **2017**
3. Yigit, C.O.; Coskun, M.Z.; Yavasoglu, H. The potential of GPS precise point positioning method for point displacement monitoring: a case study. Measurement **2016**, 91, 398-404 10.1016/j.measurement.2016.05.074
4. Chen, Q.; Jiang, W.; Meng, X.; Jiang, P.; Wang, K.; Xie, Y.; Ye, J. Vertical deformation monitoring of the suspension bridge tower Using GNSS: A Case Study of the Forth Road Bridge in the UK. *Remote Sens* **2018**, 10(3), 364-378,10.3390/rs10030364
5. Nguyen, V.H.; Schommer, S.; Maas, S.; Zürbes A. Static load testing with temperature compensation for structural health monitoring of bridges. *Eng. Struct.* **2016**, 127, 700-718, 10.1016/j.engstruct.2016.09.018
6. Chen, Z.; Guo, T.; Yan S. Life-cycle monitoring of long-span PSC box girder bridges through distributed sensor network: strategies, methods, and applications. *Shock and Vibration* **2015**, 10, 1-14, 10.1155/2015/497159
7. Lõhmus, H.; Ellmann, A.; Märdla, S.; Ldnurm, S. Terrestrial laser scanning for the monitoring of bridge load tests – two case studies. Survey Review, **2018**, 50,270-284, 10.1080/00396265.2016.1266117
8. Zhang, W; Sun L. M; and Sun, S. W. Bridge-Deflection Estimation through Inclinometer Data Considering Structural Damages. Journal of Bridge Engineering, **2017**,22(2), 04016117, 1-14 10.1061/(ASCE)BE.1943-5592.0000979
9. Xu, H.; Ren, W.X.; Wang, Z.C. Deflection estimation of bending beam structures using fiber bragg grating strain sensors. *Advances in Structural Engineering* **2015**, 18(3), 96-104,10.1260/1369-4332.18.3.395
10. Vurpillot, S., Inaudi, D., Scano, A. Mathematical model for the determination of the vertical displacement from internal horizontal measurements of a bridge. *SPIE, Smart Structures and Materials*, San Diego, USA,**1996**
11. Inaudi, D., Casanova, N., Vurpillot, S. Bridge deformation monitoring with fiber optic sensors. *IABSE Symposium*, Rio de Janeiro, Italy, **1999**
12. Cho, N.-S, Kim, N.-S. Estimating deflection of a simple beam model using fiber optic bragg-grating sensors. *Experimental Mechanics* **2004**, 44(4), 433-439, 10.1177/0014485104045431
13. Matta, F., Galati, N., Bastianini, F., Casadei, P., Nanni, A. Distributed strain and non-contact deflection measurement in multi-span highway bridge. *Proc. of the Structural Faults & Repair*, Edinburgh, UK, June 13-15, **2006**
14. Kumagai, H., Mita, A., Oka, K., Ohno, H. Development and verification of the fiber optic sensor for concrete structures. (In Japanese). *Concrete Journal* ***2000***, 38(7), 17-21
15. Shen, S.; Wu，Z; Yang, C. et.al. An improved conjugated beam method for deformation monitoring with a distributed sensitive fiber optic sensor. *Structural Health Monitoring* **2010**, 9(4), 361-378, 10.1177/1475921710361326
16. Lertsima, C; Chaisomphob, T; Yamaguchi, E and Sa-nguanmanasak, J. Deflection of simply supported box girder including effect of shear lag. *Computers and Structures* **2005**, 84, 11-18, 10.1016/j.compstruc.2005.09.008
17. Zhang, Y; Lin, L; Liu, Y. Influence of shear lag effect on deflection of box girder (in Chinese). *Chinese journal of computational mechanics* **2012**, 29(4): 625-630.
18. Zhou, W.; Jiang, L.; Liu, Z. and Liu X. Closed-form solution to thin-walled box girders considering effects of shear deformation and shear lag. *Journal of Central South University* **2012**, 19(9), 2650–2655, 10.1007/s11771-012-1323-8
19. Li, H.J.; Ye, J.S.; Song, J.Y. Influence of shear deformation on deflection of box girder with corrugated steel webs (in Chinese). *Journal of Traffic and Transportation Engineering* **2002**, 2(4), 17-20
20. Glisic,B.; Inaudi, D. Long-gage fiber optic sensors for global structural monitoring. *First International Workshop on Structural Health Monitoring of Innovative Civil Engineering Structures*, Winnipeg, Manitoba, Canada,**2002**
21. Glisic,B.; Inaudi, D. Integration of long-gage fiber-optic sensor into a fiber-reinforced composite sensing tape. *SPIE, International Symposium on Smart Structures and Materials*, San Diego, USA, **2003**

22. Li, S. and Wu, Z. Development of distributed long-gage fiber optic sensing system for structural health monitoring. *Structural Health Monitoring* **2007**, 6, 133-145, 10.1177/1475921706072078
23. Li, S. Structural health monitoring strategy based on distributed fiber optic sensing. Phd. Thesis, Ibaraki University, **2007**.
24. Hong, W.; Wu, Z.S.; Yang, C.Q. et.al. Investigation on the damage identification of bridges using distributed long-gauge dynamic macrostrain response under ambient excitation. *Journal of Intelligent Material Systems and Structures* **2012**, 23(1), 85-103, 10.1177/1045389X11430743
25. Wang, T; Tang, Y.S. Dynamic displacement monitoring of flexural structures with distributed long-gage macro-strain sensors. *Advance in mechanical engineering* **2017**, 9(4), 1-12, 10.1177/1687814017698885
26. Timoshenko, S. Strength of Materials (Part I: Elementary Theory and problems),Third Edition, Van Nostrand Reinhold Company Ltd: Molly Millars Lane, Wokingham, Berkshire, England,1955; pp. 170-175, ISBN 0-442-08539-7
27. Zhang, S. D. and Xie Q. Shear lag coefficient of box gilder and suggestion for the design code (in Chinese). *Journal of Chongqing Jiaotong University* 1986, 3, 114-128